

Article

Dielectric Responses of $(\text{Zn}_{0.33}\text{Nb}_{0.67})_x\text{Ti}_{1-x}\text{O}_2$ Ceramics Prepared by Chemical Combustion Process: DFT and Experimental Approaches

 Theeranuch Nachaithong ¹, Pairot Moontragoon ^{2,3,4,*}  and Prasit Thongbai ⁴ 
¹ Materials Science and Nanotechnology Program, Faculty of Science, Khon Kaen University, Khon Kaen 40002, Thailand

² Institute of Nanomaterials Research and Innovation for Energy (IN-RIE), Khon Kaen University, Khon Kaen 40002, Thailand

³ Thailand Center of Excellence in Physics, Commission on Higher Education, Bangkok 10400, Thailand

⁴ Department of Physics, Faculty of Science, Khon Kaen University, Khon Kaen 40002, Thailand

* Correspondence: mpauro@kku.ac.th

Abstract: The (Zn, Nb)-codoped TiO₂ (called ZNTO) nanopowder was successfully synthesized by a simple combustion process and then the ceramic from it was sintered with a highly dense microstructure. The doped atoms were consistently distributed, and the existence of oxygen vacancies was verified by a Raman spectrum. It was found that the ZNTO ceramic was a result of thermally activated giant dielectric relaxation, and the outer surface layer had a slight effect on the dielectric properties. The theoretical calculation by using the density functional theory (DFT) revealed that the Zn atoms are energy preferable to place close to the oxygen vacancy (Vo) position to create a triangle shape (called the ZnVoTi defect). This defect cluster was also opposite to the diamond shape (called the 2Nb2Ti defect). However, these two types of defects were not correlated together. Therefore, it theoretically confirms that the electron-pinned defect-dipoles (EPDD) cannot be created in the ZNTO structure. Instead, the giant dielectric property of the $(\text{Zn}_{0.33}\text{Nb}_{0.67})_x\text{Ti}_{1-x}\text{O}_2$ ceramics could be caused by the interfacial polarization combined with electron hopping between the Zn²⁺/Zn³⁺ and Ti³⁺/Ti⁴⁺ ions, rather than due to the EPDD effect. Additionally, it was also proved that the surface barrier-layer capacitor (SBLC) had a slight influence on the giant dielectric properties of the ZNTO ceramics. The annealing process can cause improved dielectric properties, which are properties with a huge advantage to practical applications and devices.

Keywords: TiO₂; electron hopping; dielectric constant; loss tangent; DFT



Citation: Nachaithong, T.; Moontragoon, P.; Thongbai, P. Dielectric Responses of $(\text{Zn}_{0.33}\text{Nb}_{0.67})_x\text{Ti}_{1-x}\text{O}_2$ Ceramics Prepared by Chemical Combustion Process: DFT and Experimental Approaches. *Molecules* **2022**, *27*, 6121. <https://doi.org/10.3390/molecules27186121>

Received: 4 August 2022

Accepted: 14 September 2022

Published: 19 September 2022

Publisher's Note: MDPI stays neutral with regard to jurisdictional claims in published maps and institutional affiliations.



Copyright: © 2022 by the authors. Licensee MDPI, Basel, Switzerland. This article is an open access article distributed under the terms and conditions of the Creative Commons Attribution (CC BY) license (<https://creativecommons.org/licenses/by/4.0/>).

1. Introduction

Recently, giant or colossal dielectric permittivity oxide materials, which are the metal oxides with a high dielectric permittivity (ϵ') (more than 10^3), e.g., BaTiO₃, CCTO, LaFeO₃ and codoped NiO-based oxides [1–7], have been extensively researched [8–15]. They have a potential to apply in many devices, i.e., multilayer ceramic capacitors and high-energy-dense storage devices. However, there are still some practical problems about their high dielectric loss tangent ($\tan\delta$) values, particularly in a range of low frequency.

In recent years, the giant dielectric properties of (In, Nb)-codoped TiO₂ ceramics (called INTO) [16] have been studied. It has been reported that codoped TiO₂ ceramics show a very high ϵ' ($\sim 10^4$), low $\tan\delta$ (~ 0.02) and high temperature stability from 80 to 450 K. However, there is still controversy in the origination of this colossal dielectric behavior. In some reports, the electron-pinned defect-dipole (EPDD) was caused by the colossal permittivity of this metal oxide. On the other hand, it was claimed that the colossal permittivity was contributed from the other effects, such as the internal barrier-layer capacitor (IBLC) effect, the surface barrier-layer capacitor (SBLC), the sample–electrode contact effect and polaronic

hopping models [16–20]. Therefore, in this work, the mechanics inside of the giant dielectric permittivity of TiO₂-based ceramics will be reported and clarified. Although the colossal dielectric response of (Zn, Nb)-codoped TiO₂ was widely investigated [21,22], the colossal permittivity properties of these system ceramics synthesized by wet chemical routes has not been widely reported. Thus, in this study, both experimental and theoretical studies were simultaneously performed on TiO₂ ceramics codoped with Zn²⁺/Nb⁵⁺ ions. In the experimental part, both the (Zn_{0.33}Nb_{0.67})_xTi_{1-x}O₂ powders and sintered ceramics were thoroughly fabricated and characterized. Their colossal permittivity properties at different frequencies and temperatures were investigated to expose the mechanics and behavior inside the microstructures. In the theoretical aspect, the density functional theory (DFT) was employed to evaluate the ground-state properties of the (Zn_{0.33}Nb_{0.67})_xTi_{1-x}O₂ to understand the cause of the colossal permittivity in the (Zn, Nb)-codoped TiO₂ ceramics. The feasible explanation for the noticed giant permittivity behavior will be reported.

2. Experimental Details

(Zn_{0.33}Nb_{0.67})_xTi_{1-x}O₂ (ZNTO) nanoparticles ($x = 0.5, 1, 2.5, 5.0$ and 10%) were synthesized by a simple combustion method. C₁₆H₂₈O₆Ti (Sigma-Aldrich, Bangkok, Thailand), NbCl₅ (Sigma-Aldrich, >99.9%), N₂O₆Zn·xH₂O (Sigma-Aldrich, 99.999%) were weighed corresponding to each doped content. Firstly, NbCl₅ and N₂O₆Zn·xH₂O were mixed in citric acid and then a C₁₆H₂₈O₆Ti solution was mixed at 130 °C and stirred until a gel was obtained. Secondly, all doping concentrations gels were calcined, then they were pressed into pellets with diameter of 9.5 mm and thickness of ~1.3 mm. Finally, they were sintered at 1400 °C for 5 h. (Zn_{0.33}Nb_{0.67})_xTi_{1-x}O₂ ceramics with $x = 0.5$ and 0.25% are referred to as the 0.5% ZNTO and 2.5% ZNTO ceramics, respectively.

The phase structure of all samples was characterized by X-ray diffraction technique (XRD, PANalytical, EMPYREAN). The field emission scanning electron microscopy technique (FE-SEM, FEI, Hileos Nanolab G3CX) was performed to reveal the surface morphologies of the homogeneity of all elements in the sintered samples. To confirm existing oxygen vacancies in the microstructures, the Raman spectra of sintered ceramics were measured with a Raman System (NT-MDT Ntegra Spectra), using laser wavelength of 532 nm. Finally, the dielectric properties or permittivity responses were measured by an impedance analyzer technique (KEYSIGHT E4990A). In this study, the temperature dependence of the dielectric constant (ϵ') and loss tangent ($\tan\delta$) was measured in the frequency and temperature ranges of 10²–10⁶ Hz and –60 to 200 °C. In order to thoroughly understand inside the nanoscale level, the stable configuration of the periodic boundary conditions of 2 × 2 × 6 super-cell Zn and Nb-codoped rutile-TiO₂ structure was studied using the DFT calculation, performed under Vienna Ab initio Simulation Package (VASP) with Projector-augmented plane-wave pseudopotential method (PAW) and the Perdew–Burke–Ernzerhof (PBE) form of exchange–correlation functional. In this model, firstly, one oxygen vacancy was created and then replaced two Ti atoms with Zn atoms to form 2ZnVo triangular defect and another two Ti atoms with Nb atoms to form 2NbTi diamond defect. Additionally, cutoff energy of 600 eV and 3 × 3 × 3 k-point meshes in Monkhorst–Pack k-point are also employed to optimize the structures to obtain the lowest energy-preferable configuration, the conjugate-gradient algorithm and Hellmann–Feynman theorem were carried out to calculate the force acting on each ion and 5 × 5 × 5 k-point meshes in Monkhorst–Pack k-point are used to calculate the electronic structures. The orbitals of Ti(3p⁶ 4s² 3d²), Zn(3p⁶ 4s² 3d¹⁰), O(2s² 2p⁴) and Nb(4p⁶ 5s¹ 4d⁴) were treated as valence electrons.

3. Results and Discussion

According to Figure 1, the XRD patterns of the ZNTO powders prepared by a chemical combustion method confirmed the rutile-TiO₂ (JCPDS 21-1276) [23,24] phase and no impurity phase, which is in good agreement with other works [23–25]. The a and c values, extracted from the XRD patterns, are shown in Table 1, and they increased with the rising doping content. These results confirmed that the Zn²⁺ and Nb⁵⁺ can substitute in the Ti

sites of the rutile structure of TiO_2 . The increase in the lattice parameters was due to the larger ionic radii of the dopants compared to that of the Ti^{4+} host ion.

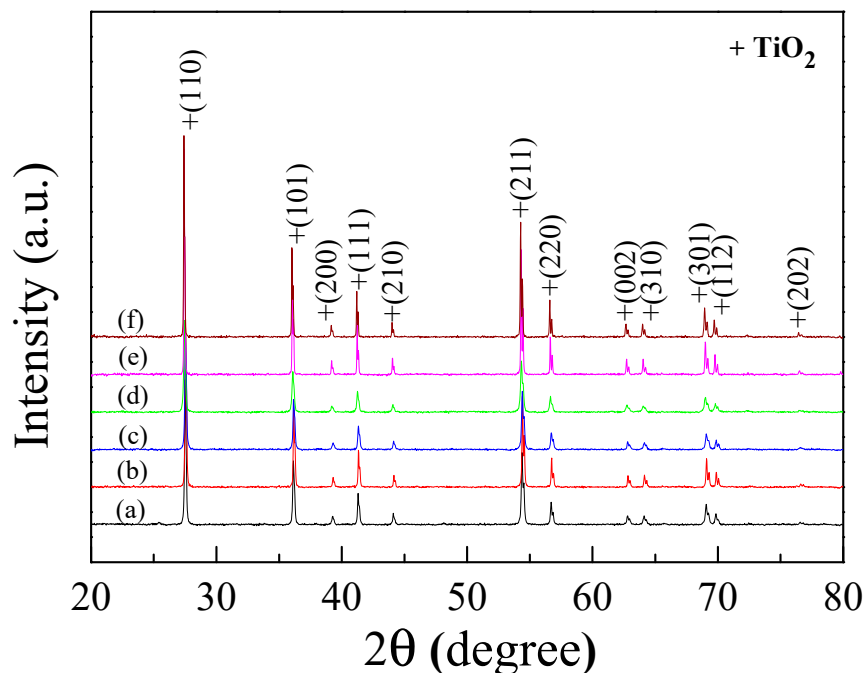


Figure 1. XRD patterns of single doped (a) Zn, (b) Nb in TiO_2 powder and $(\text{Zn}_{0.33}\text{Nb}_{0.67})_x\text{Ti}_{1-x}\text{O}_2$ powder with $x =$ (c) 0.5%, (d) 2.5% and (e) 0.5% ZNTO, (f) 2.5% ZNTO ceramics.

Table 1. Lattice parameter of ZNTO powders and ceramics with difference codoping levels.

	Sample	Lattice Parameter (Å)	
		<i>a</i>	<i>c</i>
(a)	0.5% Zn- TiO_2 powder	4.5961	2.9618
(b)	0.5% Nb- TiO_2 powder	4.5964	2.9619
(c)	$(\text{Zn}_{0.33}\text{Nb}_{0.67})_x\text{Ti}_{1-x}\text{O}_2$ powder with $x = 0.5\%$	4.5971	2.9621
(d)	$(\text{Zn}_{0.33}\text{Nb}_{0.67})_x\text{Ti}_{1-x}\text{O}_2$ powder with $x = 2.5\%$	4.5994	2.9624
(e)	0.5% ZNTO	4.5967	2.9625
(f)	2.5% ZNTO	4.5997	2.9647

According to Figure 2, the surface morphologies of the ZNTO ceramic sintered at 1400°C for 5 h with 0.5 and 2.5% were revealed. It shows that the grains with grain sizes of 5.7 ± 2.4 and $3.7 \pm 1.3 \mu\text{m}$, respectively, and the grain boundaries were clearly observed. The microstructure of the sintered ceramics was highly dense without pores in the 0.5% ZNTO and 2.5% ZNTO ceramics. The mean grain size of the ZNTO ceramics decreased with an increasing codoping concentration. This result is similar to those reported in the literature by Nachaithong et al. [26] and Yang et al. [27]. It was explained that the decreased mean grain size of the codoped TiO_2 ceramics was caused by the solute drag mechanism.

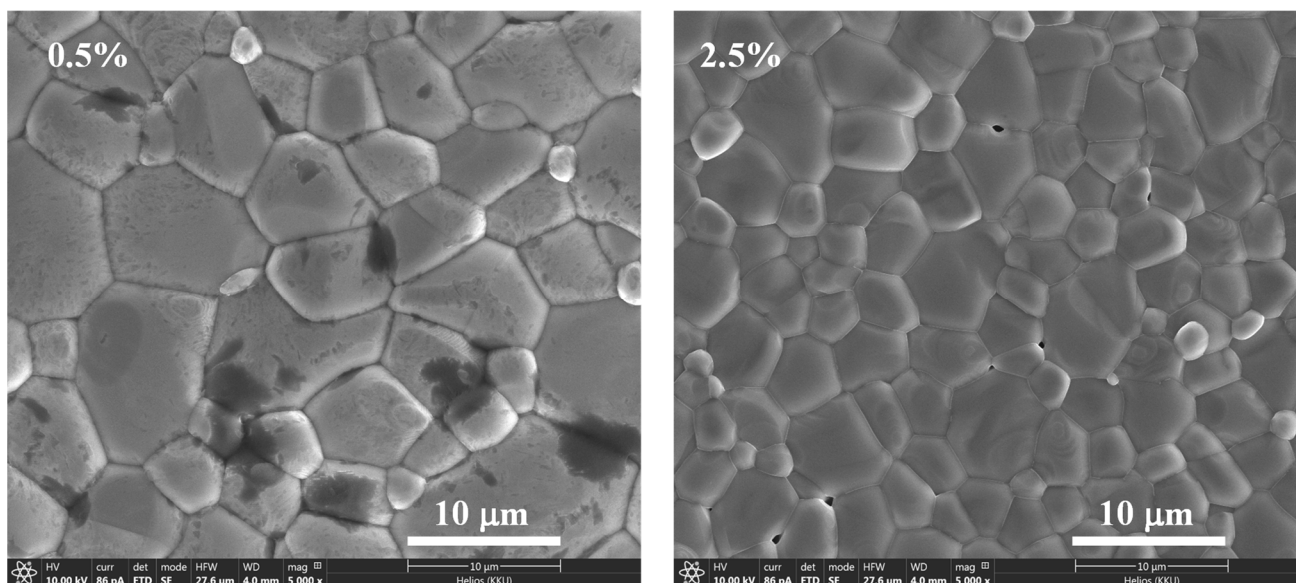


Figure 2. Surface morphologies of the $(\text{Zn}_{0.33}\text{Nb}_{0.67})_x\text{Ti}_{1-x}\text{O}_2$ ceramics with $x = 0.5$ and 2.5% .

As shown in Figure 3, the Raman spectra of the pure TiO_2 and ZNTO ceramics with the E_g and A_{1g} modes were presented. The E_g peaks of the TiO_2 , 0.5% Nb-doped TiO_2 , 0.5% Zn-doped TiO_2 , 0.5% ZNTO and 2.5% ZNTO samples appeared at 446.5 , 446.5 , 446.5 , 444.5 and 444.5 cm^{-1} , respectively, whereas the A_{1g} modes appeared at 610.5 , 610.0 , 611.0 , 611.5 and 610.5 cm^{-1} , respectively. It was shown that the oxygen vacancies and O–Ti–O bonds were associated with the E_g and A_{1g} modes [28].

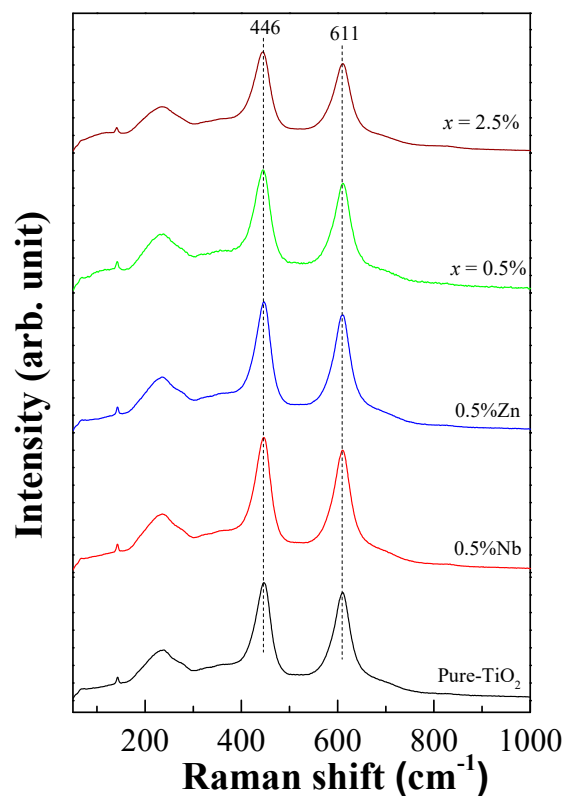


Figure 3. Raman spectra of rutile- TiO_2 , single doped of Nb^{5+} and Zn^{2+} and ZNTO ceramics with difference codoping levels.

According to Figure 4, the SEM-mapping method was used to reveal a distribution of the elements in the ZNTO ceramics (such as Zn, Nb, Ti and O), and it was found that there is a homogeneous dispersion of the doped elements in the microstructure.

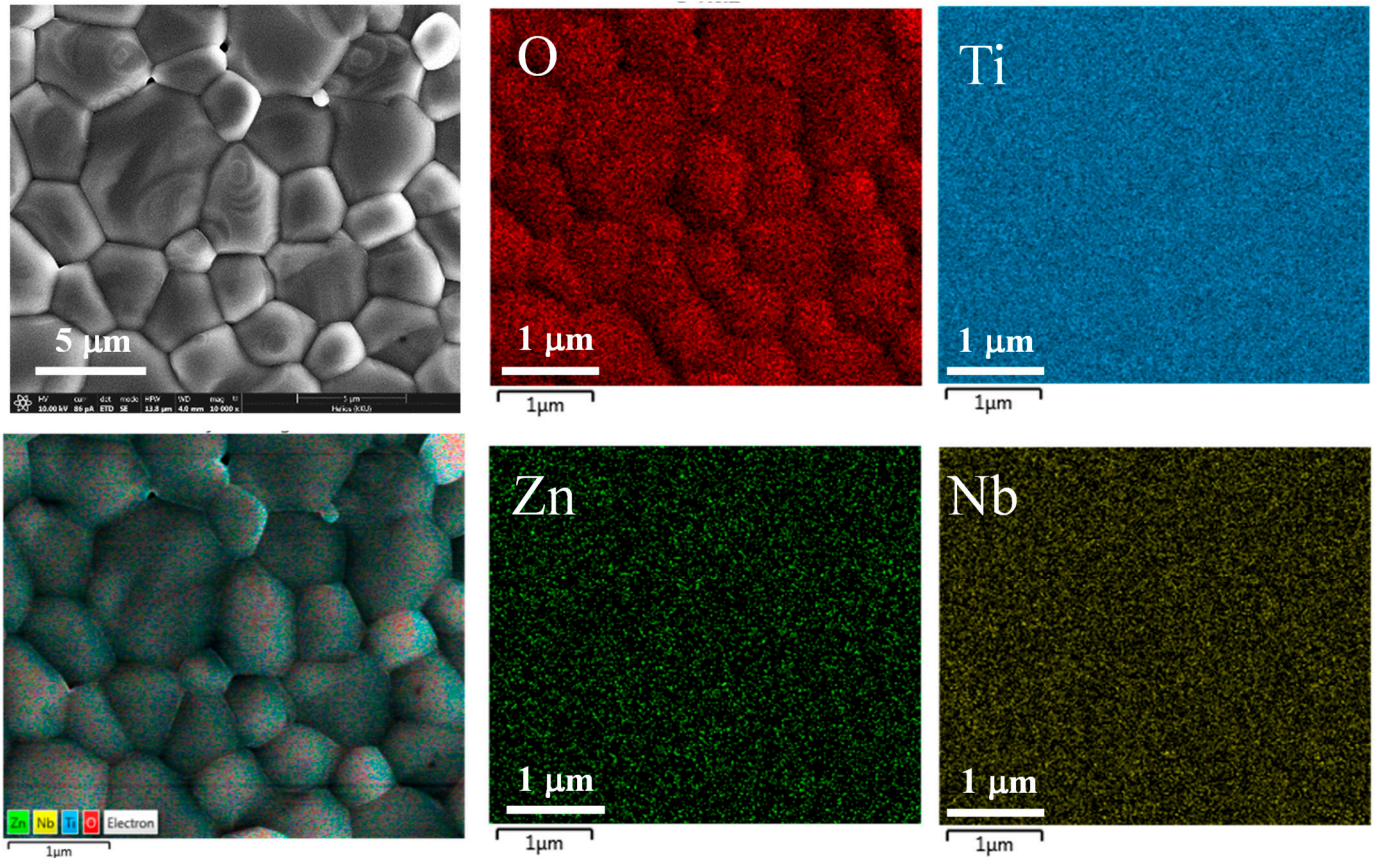


Figure 4. The elements mapping of 2.5% ZNTO ceramic; the Zn, Nb, Ti and O dopants are homogeneously dispersed in the grains and grain boundaries.

Figure 5 shows the ϵ' permittivity at room temperature of the Pure-TiO₂, 0.5% ZNTO and 2.5% ZNTO ceramics. All the samples exhibited a giant dielectric permittivity in the frequency range of 40–10⁶ Hz. The ϵ' value of a pure-TiO₂ was the lowest. Although a rutile-TiO₂ had the largest ϵ' value among the simple oxides, its ϵ' value is very low compared to those of many complex oxides, such as BaTiO₃ and CaCu₃Ti₄O₁₂-based materials. Nevertheless, the ϵ' value of TiO₂ can be significantly enhanced by codoping metal ions. In the $\tan\delta$ spectrum, the samples showed that the $\tan\delta$ peaks in the frequency range of 10³–10⁴ and ϵ' slightly changed. This dielectric relaxation behavior could imply that the Nb⁵⁺ and Zn²⁺ codoping ions have slightly affected the ionic polarization. However, when it was considered in a low-frequency range, the $\tan\delta$ increased with an increasing codopant concentration. It shows that the codopants have an effect on the interfacial polarization which is usually induced at the internal insulating layer, i.e., a semiconducting region or surface of the sample–electrode layer of ceramics. The ϵ' values of the 0.5% ZNTO and 2.5% ZNTO ceramics were about $\approx 9 \times 10^4$ and 3×10^4 with $\tan\delta \approx 0.26$ and 1.25 at 1 kHz and RT, respectively.

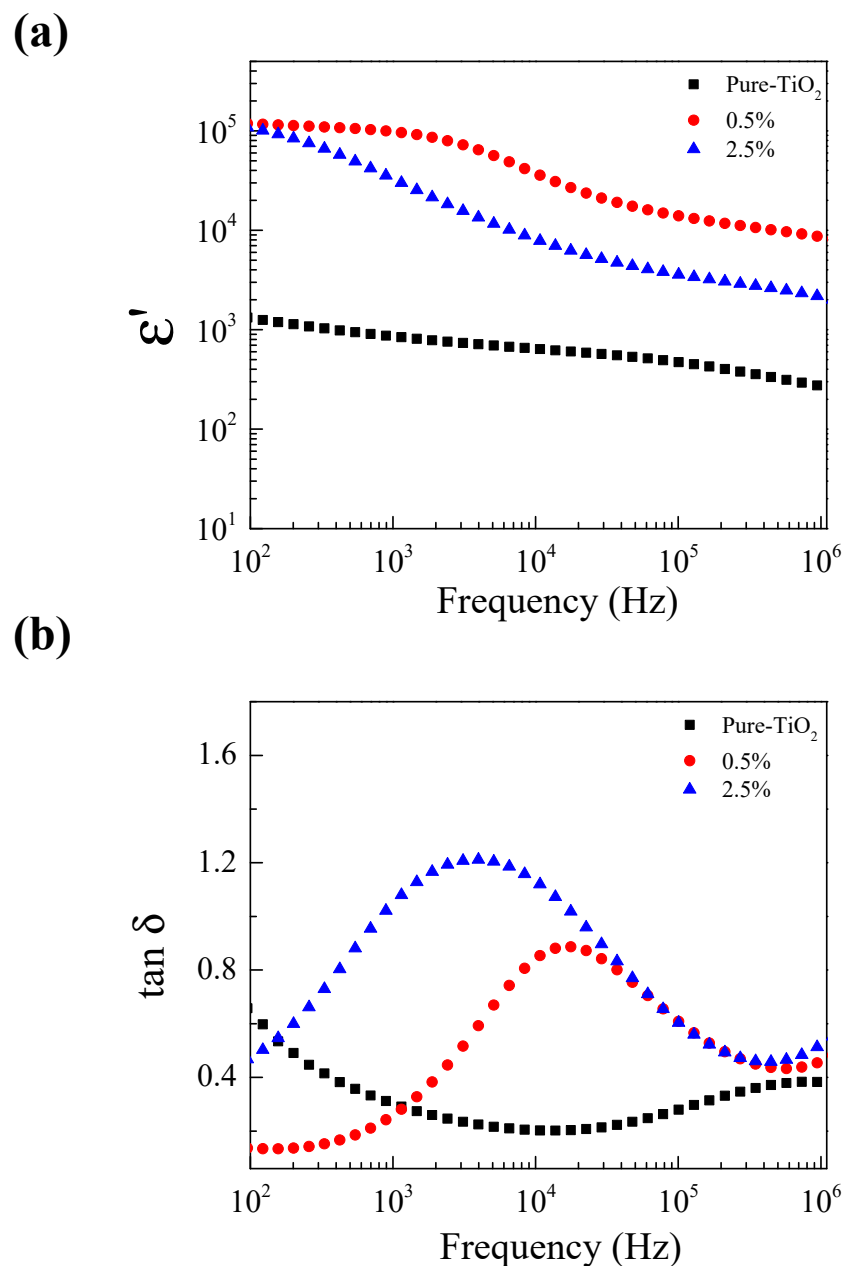
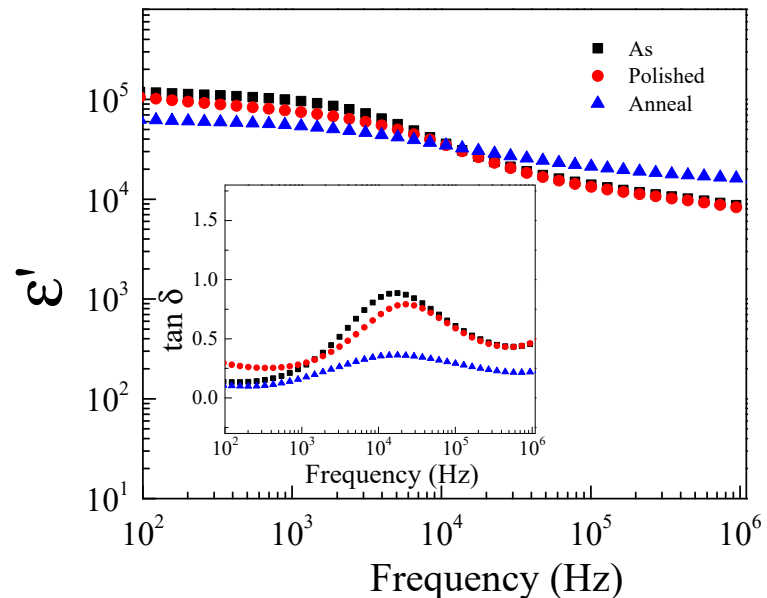


Figure 5. Frequency dependence of (a) ϵ' and (b) $\tan \delta$ at RT for ZNTO ceramics with various codopant concentrations ($x = 0.5\%$, 0.25%).

To study the effects of the surface on the electrical properties of ZNTO ceramics in Figure 6, after the dielectric properties of the as-fired sample were measured, both sides of the electrodes and the outer surface layers of the pellet were removed by polishing them with SiC paper (referred to as the polished-sample), and after that, the polished-sample was measured, the electrodes were removed by the SiC paper and annealed at 1200 °C in air for 30 min (referred to as the annealed-sample). In comparison with the as-sample, polished-sample and annealed-sample, at room temperature, all the samples exhibited very high ϵ' values of $\approx 10^4$ – 10^5 . The change in the ϵ' and $\tan \delta$ was not considerable compared with that of the polished-sample, but the dielectric permittivity slightly increased in frequency, more than 10^3 Hz. The $\tan \delta$ decreased significantly when compared with the as-sample. After the annealing process, the greatly reduced $\tan \delta$ value and greatly increased ϵ' value in the anneal-sample were primarily due to the filling of the oxygen vacancies on the surface. Therefore, the SBLC effect was a key factor for the anneal-sample. In this experiment, it

was clearly shown that the outer surface layer influences the dielectric responses of the ZNTO ceramics. The annealing method was suggested to be one of the most important for the improvement of the dielectric properties of ZNTO ceramics by creating a resistive outer surface layer. Furthermore, this method could be a new outer surface design approach for other codoped TiO₂ ceramic systems.

(a)



(b)

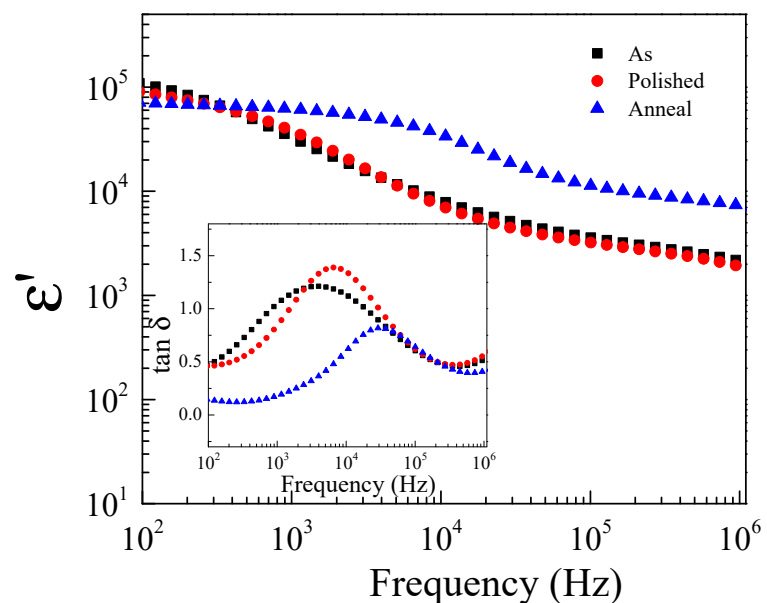


Figure 6. Frequency dependence of ϵ' at RT of the as-fired sample, polished-sample and annealed-sample (in air) for $(\text{Zn}_{0.33}\text{Nb}_{0.67})_x\text{Ti}_{1-x}\text{O}_2$ ceramics with $x = 0.5\%$ (a), 2.5% (b); inset shows frequency dependence of $\tan\delta$ at RT.

To explain the behavior of the colossal dielectric properties in ZNTO ceramics, the effect of temperature on the dielectric behavior at different frequencies and temperatures was investigated, as shown in Figure 7. It is seen that the ϵ' step likely decreases with an increasing frequency, but increases with an increasing temperature, corresponding to

a decrease in the resistance (R). Moreover, the corresponding $\tan\delta$ peak also increases. This confirmed the thermally activated giant dielectric relaxation behavior. According to Figure 8, the Arrhenius plots of the 0.5% ZNTO and 2.5% ZNTO ceramics show the activation energy (E_a) which is the temperature dependence of the relaxation peak of the dielectric loss (f_{\max}), following the Arrhenius law:

$$f_{\max} = f_0 \exp\left(\frac{-E_a}{K_B T}\right) \quad (1)$$

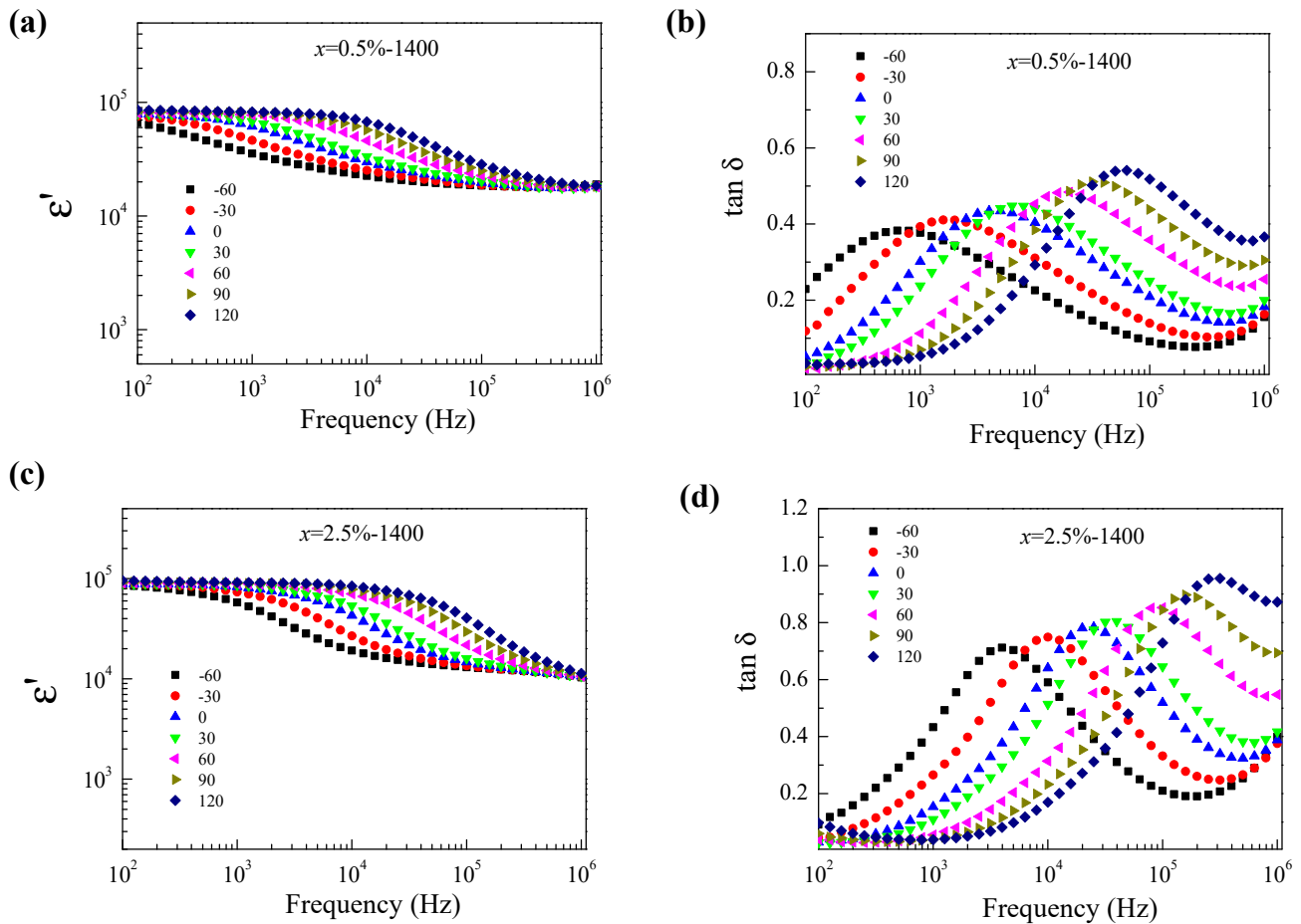
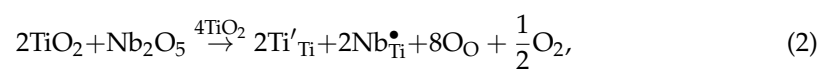


Figure 7. Temperature dependence of the (a,c) dielectric relaxation and (b,d) $\tan\delta$ at different frequencies for ZNTO ceramics with $x = 0.5$ and 2.5% respectively.

It is required energy for the dielectric relaxation in the ceramics and calculated from the slope of the $\ln f_{\max}$ vs. $1000/T$ plots. The E_a values of the 0.5% ZNTO and 2.5% ZNTO ceramics were 0.213 and 0.175 eV, respectively. It is implied that the giant dielectric response could be related to the Zn^{2+}/Zn^{3+} or Ti^{3+}/Ti^{4+} electron hopping. Increasing the Nb^{5+} doping concentration could result in a Ti^{3+}/Ti^{4+} ions ratio increase. The concentration of the free electrons in the Nb^{5+} -doped TiO_2 is generally proportional to the Nb^{5+} dopant concentration, following the equations [16]:



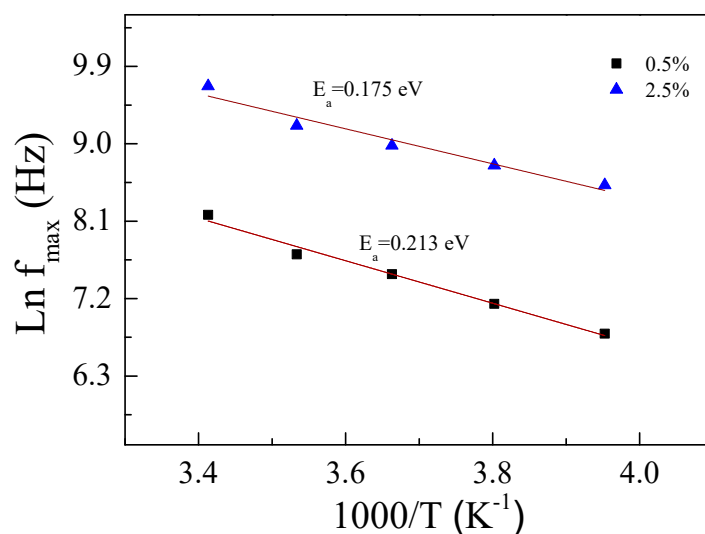


Figure 8. Arrhenius plots of the dielectric relaxation process for 0.5% and 2.5% ZNTO ceramics.

Therefore, the electron hopping can be readily stimulated when the Ti^{3+} or Zn^{3+} content rises, giving rise to a decrease in the E_a values for the ZNTO ceramics with $x = 0.5$ and 2.5%.

According to the theoretical investigations, we placed 2Nb atoms preferentially forming a diamond-shaped structure (called 2Nb2Ti defect) and the 2ZnVo triangular defect into the TiO_2 structure simultaneously in three configurations: near, opposite and far. The lowest total energy can be obtained when the 2Nb diamond defects and 2ZnVo triangular defects are opposite (as shown in Figure 9), corresponding to the EPDD model and not in the ZNTO structure. It can be clearly suggested that the giant dielectric relaxation behavior of the ZNTO ceramics did not originate from the EPDD effect. Moreover, the electron hopping mechanism between the $\text{Ti}^{3+}/\text{Ti}^{4+}$ ions and $\text{Zn}^{2+}/\text{Zn}^{3+}$ is also the most likely mechanism to be related to the giant dielectric relaxation in the ZNTO ceramics.

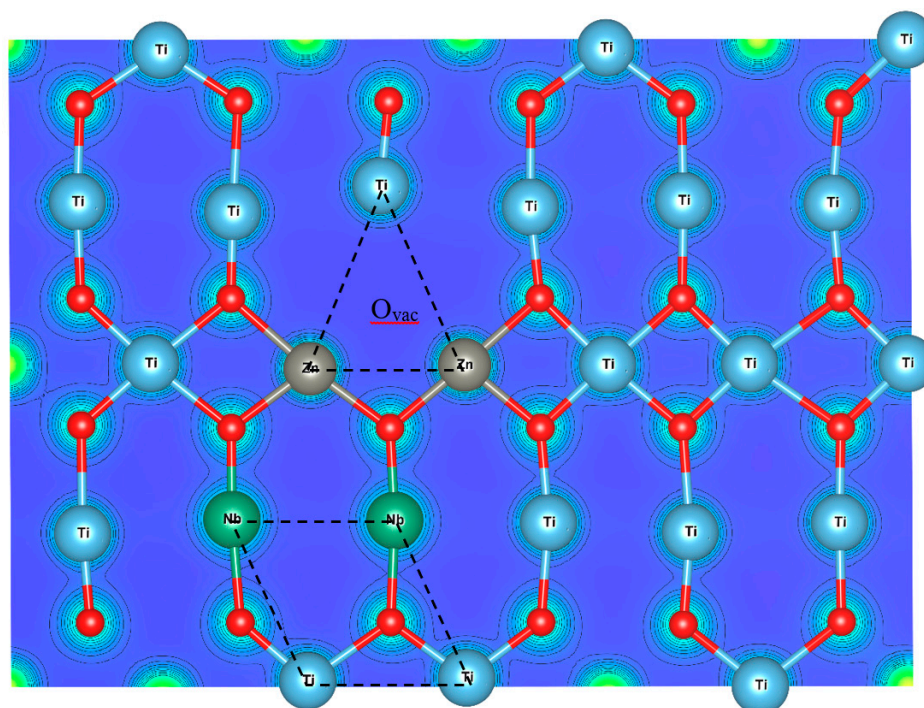


Figure 9. Energy-preferable structure of the 2ZnVo triangular defect and 2Nb diamond defect.

4. Conclusions

In this work, the (Zn + Nb)-codoped TiO₂ ceramics prepared by a combustion process show a colossal dielectric permittivity and a low loss behavior. Moreover, their dielectric characteristics show a good frequency stability. The annealing process can cause improved dielectric properties, which are properties with a huge advantage in practical applications and devices. In addition, the giant dielectric relaxation behavior of the ZNTO originated from both the IBLC and the Ti³⁺/Ti⁴⁺ ions and Zn²⁺/Zn³⁺ electron hopping mechanism. It indicates that there is giant dielectric relaxation behavior in the (Zn, Nb)-codoped TiO₂ systems.

Author Contributions: Conceptualization, P.T. and P.M.; methodology, T.N.; software, T.N.; validation, T.N., P.M. and P.T.; formal analysis, T.N.; investigation, T.N.; resources, T.N.; data curation, T.N.; writing—original draft preparation, T.N.; writing—review and editing, P.M.; visualization, P.M.; supervision, P.M.; project administration, P.M.; funding acquisition, P.T. All authors have read and agreed to the published version of the manuscript.

Funding: The Fundamental Fund Khon Kaen University, the Basic Research Fund of Khon Kaen University, the National Research Council of Thailand (NRCT) and Khon Kaen University: N42A650294. Thailand Research Fund under The Royal Golden Jubilee Ph.D. Program [Grant Number PHD/0114/2559].

Institutional Review Board Statement: Not Applicable.

Informed Consent Statement: Not Applicable.

Data Availability Statement: The study did not report any data.

Acknowledgments: T. Nachaithong would like to thank the Thailand Research Fund under The Royal Golden Jubilee Ph.D. Program [Grant Number PHD/0114/2559] for his Ph.D. scholarship.

Conflicts of Interest: The authors declare no conflict of interest.

References

1. Wu, J.; Nan, C.W.; Lin, Y.; Deng, Y. Giant dielectric permittivity observed in Li and Ti doped NiO. *Phys. Rev. Lett.* **2002**, *89*, 217601. [[CrossRef](#)] [[PubMed](#)]
2. Schmidt, R.; Stennett, M.C.; Hyatt, N.C.; Pokorny, J.; Prado-Gonjal, J.; Li, M.; Sinclair, D.C. Effects of sintering temperature on the internal barrier layer capacitor (IBLC) structure in CaCu₃Ti₄O₁₂ (CCTO) ceramics. *J. Eur. Ceram. Soc.* **2012**, *32*, 3313–3323. [[CrossRef](#)]
3. Liu, L.; Fan, H.; Fang, P.; Chen, X. Sol-gel derived CaCu₃Ti₄O₁₂ ceramics: Synthesis, characterization and electrical properties. *Mater. Res. Bull.* **2008**, *43*, 1800–1807. [[CrossRef](#)]
4. Li, J.; Wu, K.; Jia, R.; Hou, L.; Gao, L.; Li, S. Towards enhanced varistor property and lower dielectric loss of CaCu₃Ti₄O₁₂ based ceramics. *Mater. Des.* **2016**, *92*, 546–551. [[CrossRef](#)]
5. Xu, T.; Wang, C.-A. Effect of two-step sintering on micro-honeycomb BaTiO₃ ceramics prepared by freeze-casting process. *J. Eur. Ceram. Soc.* **2016**, *36*, 2647–2652. [[CrossRef](#)]
6. Liu, Y.; Wang, W.; Huang, J.; Zhu, C.; Wang, C.; Cao, Y. High dielectric permittivity of Li and Sc co-doped NiO ceramics. *J. Mater. Sci. Mater. Electron.* **2014**, *25*, 1298–1302. [[CrossRef](#)]
7. Ni, W.; Ye, J.; Guo, Y.; Cheng, C.; Lin, Z.; Li, Y.; Wang, H.; Yu, Y.; Li, Q.; Huang, S.; et al. Decisive role of mixed-valence structure in colossal dielectric constant of LaFeO₃. *J. Am. Ceram. Soc.* **2017**, *100*, 3042–3049. [[CrossRef](#)]
8. Ni, L.; Chen, X.M. Dielectric relaxations and formation mechanism of giant dielectric constant step in CaCu₃Ti₄O₁₂ ceramics. *Appl. Phys. Lett.* **2007**, *91*, 122905. [[CrossRef](#)]
9. Ke, S.; Fan, H.; Huang, H. Dielectric relaxation in A₂FeNbO₆ (A = Ba, Sr, and Ca) perovskite ceramics. *J. Electroceramics* **2009**, *22*, 252–256. [[CrossRef](#)]
10. Zhang, C.-h.; Zhang, K.; Xu, H.-x.; Song, Q.; Yang, Y.-t.; Yu, R.-h.; Xu, D.; Cheng, X.-n. Microstructure and electrical properties of sol-gel derived Ni-doped CaCu₃Ti₄O₁₂ ceramics. *Trans. Nonferrous Met. Soc. China* **2012**, *22*, s127–s132. [[CrossRef](#)]
11. Shi, Y.; Hao, W.; Wu, H.; Sun, L.; Cao, E.; Zhang, Y.; Peng, H. High dielectric-permittivity properties of NaCu₃Ti₃Sb_{0.5}Nb_{0.5}O₁₂ ceramics. *Ceram. Int.* **2015**, *42*, 116–121. [[CrossRef](#)]
12. Wang, Z.; Cao, M.; Zhang, Q.; Hao, H.; Yao, Z.; Wang, Z.; Song, Z.; Zhang, Y.; Hu, W.; Liu, H. Dielectric Relaxation in Zr-Doped SrTiO₃ Ceramics Sintered in N₂ with Giant Permittivity and Low Dielectric Loss. *J. Am. Ceram. Soc.* **2015**, *98*, 476–482. [[CrossRef](#)]
13. Liu, Y.; Zhao, X.; Zhang, C. Dielectric and impedance characteristics of Na_{1/3}Ca_{1/3}Y_{1/3}Cu₃Ti₄O₁₂ ceramic prepared by solid-state reaction method. *J. Mater. Sci. Mater. Electron.* **2016**, *27*, 11757–11761. [[CrossRef](#)]
14. Nautiyal, A.; Autret, C.; Honstetter, C.; De Almeida-Didry, S.; Amrani, M.E.; Roger, S.; Negulescu, B.; Ruyter, A. Local analysis of the grain and grain boundary contributions to the bulk dielectric properties of Ca(Cu_{3-y}Mg_y)Ti₄O₁₂ ceramics: Importance of the potential barrier at the grain boundary. *J. Eur. Ceram. Soc.* **2016**, *36*, 1391–1398. [[CrossRef](#)]

15. Jumpatam, J.; Thongbai, P.; Yamwong, T.; Maensiri, S. Effects of Bi³⁺ doping on microstructure and dielectric properties of CaCu₃Ti₄O₁₂/CaTiO₃ composite ceramics. *Ceram. Int.* **2015**, *41*, S498–S503. [[CrossRef](#)]
16. Hu, W.; Liu, Y.; Withers, R.L.; Frankcombe, T.J.; Noren, L.; Snashall, A.; Kitchin, M.; Smith, P.; Gong, B.; Chen, H.; et al. Electron-pinned defect-dipoles for high-performance colossal permittivity materials. *Nat. Mater.* **2013**, *12*, 821–826. [[CrossRef](#)]
17. Nachaithong, T.; Kidkhunthod, P.; Thongbai, P.; Maensiri, S. Surface barrier layer effect in (In + Nb) co-doped TiO₂ ceramics: An alternative route to design low dielectric loss. *J. Am. Ceram. Soc.* **2017**, *100*, 1452–1459. [[CrossRef](#)]
18. Li, J.; Li, F.; Zhuang, Y.; Jin, L.; Wang, L.; Wei, X.; Xu, Z.; Zhang, S. Microstructure and dielectric properties of (Nb + In) co-doped rutile TiO₂ ceramics. *J. Appl. Phys.* **2014**, *116*, 074105. [[CrossRef](#)]
19. Zhang, L.; Tang, Z.-J. Polaron relaxation and variable-range-hopping conductivity in the giant-dielectric-constant material CaCu₃Ti₄O₁₂. *Phys. Rev. B* **2004**, *70*, 174306. [[CrossRef](#)]
20. Lunkenheimer, P.; Fichtl, R.; Ebbinghaus, S.; Loidl, A. Nonintrinsic origin of the colossal dielectric constants in CaCu₃Ti₄O₁₂. *Phys. Rev. B* **2004**, *70*, 172102. [[CrossRef](#)]
21. Wei, X.; Jie, W.; Yang, Z.; Zheng, F.; Zeng, H.; Liu, Y.; Hao, J. Colossal permittivity properties of Zn,Nb co-doped TiO₂ with different phase structures. *J. Mater. Chem. C* **2015**, *3*, 11005–11010. [[CrossRef](#)]
22. Thongyong, N.; Tuichai, W.; Chanlek, N.; Thongbai, P. Effect of Zn²⁺ and Nb⁵⁺ co-doping ions on giant dielectric properties of rutile-TiO₂ ceramics. *Ceram. Int.* **2017**, *43*, 15466–15471. [[CrossRef](#)]
23. Nachaithong, T.; Thongbai, P.; Maensiri, S. Colossal permittivity in (In_{1/2}Nb_{1/2})_xTi_{1-x}O₂ ceramics prepared by a glycine nitrate process. *J. Eur. Ceram. Soc.* **2017**, *37*, 655–660. [[CrossRef](#)]
24. Zhu, X.; Yang, L.; Li, J.; Jin, L.; Wang, L.; Wei, X.; Xu, Z.; Li, F. The dielectric properties for (Nb,In,B) co-doped rutile TiO₂ ceramics. *Ceram. Int.* **2017**, *43*, 6403–6409. [[CrossRef](#)]
25. Zhang, J.; Yue, Z.; Zhou, Y.; Peng, B.; Zhang, X.; Li, L. Temperature-dependent dielectric properties, thermally-stimulated relaxations and defect-property correlations of TiO₂ ceramics for wireless passive temperature sensing. *J. Eur. Ceram. Soc.* **2016**, *36*, 1923–1930. [[CrossRef](#)]
26. Nachaithong, T.; Tuichai, W.; Kidkhunthod, P.; Chanlek, N.; Thongbai, P.; Maensiri, S. Preparation, characterization, and giant dielectric permittivity of (Y³⁺ and Nb⁵⁺) co-doped TiO₂ ceramics. *J. Eur. Ceram. Soc.* **2017**, *37*, 3521–3526. [[CrossRef](#)]
27. Yang, C.; Wei, X.; Hao, J. Disappearance and recovery of colossal permittivity in (Nb+Mn) co-doped TiO₂. *Ceram. Int.* **2018**, *11*, 12395–12400. [[CrossRef](#)]
28. Hu, W.; Lau, K.; Liu, Y.; Withers, R.L.; Chen, H.; Fu, L.; Gong, B.; Hutchison, W. Colossal Dielectric Permittivity in (Nb+Al) Codoped Rutile TiO₂ Ceramics: Compositional Gradient and Local Structure. *Chem. Mater.* **2015**, *27*, 4934–4942. [[CrossRef](#)]